


Brain atrophy progression in Parkinson's disease is shaped by connectivity and local vulnerability

Christina Tremblay,¹  Shady Rahayel,^{1,2} Andrew Vo,¹ Filip Morys,¹  Golia Shafiei,¹  Nooshin Abbasi,¹  Ross D. Markello,¹  Ziv Gan-Or,^{1,3}  Bratislav Mistic¹ and  Alain Dagher¹

Brain atrophy has been reported in the early stages of Parkinson's disease, but there have been few longitudinal studies. How intrinsic properties of the brain, such as anatomical connectivity, local cell-type distribution and gene expression combine to determine the pattern of disease progression also remains unknown. One hypothesis proposes that the disease stems from prion-like propagation of misfolded alpha-synuclein via the connectome that might cause varying degrees of tissue damage based on local properties. Here, we used MRI data from the Parkinson Progression Markers Initiative to map the progression of brain atrophy over 1, 2 and 4 years compared with baseline. We derived atrophy maps for four time points using deformation-based morphometry applied to T₁-weighted MRI from 120 *de novo* Parkinson's disease patients, 74 of whom had imaging at all four time points (50 Men: 24 Women) and 157 healthy control participants (115 Men: 42 Women). In order to determine factors that may influence neurodegeneration, we related atrophy progression to brain structural and functional connectivity, cell-type expression and gene ontology enrichment analyses. After regressing out the expected age and sex effects associated with normal ageing, we found that atrophy significantly progressed over 2 and 4 years in the caudate, nucleus accumbens, hippocampus and posterior cortical regions. This progression was shaped by both structural and functional brain connectivity. Also, the progression of atrophy was more pronounced in regions with a higher expression of genes related to synapses and was inversely related to the prevalence of oligodendrocytes and endothelial cells. In sum, we demonstrate that the progression of atrophy in Parkinson's disease is in line with the prion-like propagation hypothesis of alpha-synuclein and provide evidence that synapses may be especially vulnerable to synucleinopathy. In addition to identifying vulnerable brain regions, this study reveals different factors that may be implicated in the neurotoxic mechanisms leading to progression in Parkinson's disease. All brain maps generated here are available on request.

1 Montreal Neurological Institute, McGill University, Montreal, QC H3A 2B4, Canada

2 Centre for Advanced Research in Sleep Medicine, Hôpital du Sacré-Cœur de Montréal, Montreal, QC H4J 1C5, Canada

3 Department of Human Genetics, McGill University, Montreal, QC H3A 0C7, Canada

Correspondence to: Alain Dagher, MD
Montreal Neurological Institute and Hospital
3801 University Street, Montreal
QC H3A 2B4, Canada
E-mail: alain.dagher@mcgill.ca

Keywords: Parkinson's disease; atrophy progression; deformation-based morphometry; connectivity; cell types

Received March 26, 2021. Revised August 18, 2021. Accepted October 18, 2021. Advance Access publication November 17, 2021

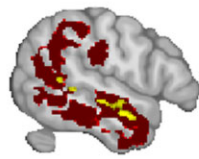
© The Author(s) (2021). Published by Oxford University Press on behalf of the Guarantors of Brain.

This is an Open Access article distributed under the terms of the Creative Commons Attribution License (<https://creativecommons.org/licenses/by/4.0/>), which permits unrestricted reuse, distribution, and reproduction in any medium, provided the original work is properly cited.

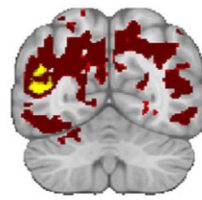
Abbreviations: AHBA = Allen Human Brain Atlas; BBB = blood–brain barrier; Bl = baseline; CAT12 = Computational Anatomy Toolbox; DBM = deformation-based morphometry; FC = functional connectivity; FDR = false discovery rate; FEW = Family-wise error; GDS = Geriatric Depression Scale; GO = gene ontology; GOrilla = Gene Ontology enRICHment anaLysis and visuaLizAtion tool; HC = healthy control; HVLt = Hopkins Verbal Learning Test; L-Dopa = Levodopa; MDS-UPDRS = Movement Disorder Society Unified Parkinson Disease Rating Scale; MNI = Montreal Neurological Institute; MoCA = Montreal Cognitive Assessment; NFL = neurofilament light polypeptide; PPMI = Parkinson’s progression markers initiative; pTFCE = probabilistic approach for threshold-free cluster enhancement; SD = standard deviation; SPM12 = Statistical Parametric Mapping software; STAI = State-Trait Anxiety Inventory

Graphical Abstract

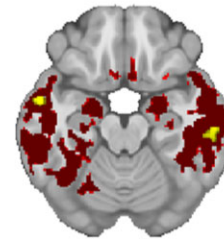
Atrophy progression after 2 (yellow) and 4 years (red) in *de novo* Parkinson’s disease



$x = 54$



$y = -62$

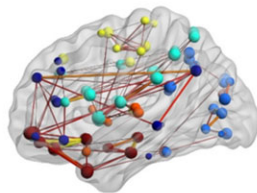


$z = -19$

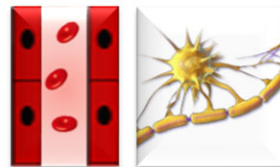
RELATED TO



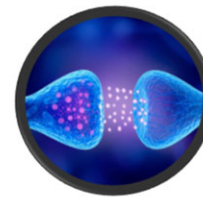
Structural and Functional Connectivity



Endothelial cells and Oligodendrocytes



Synaptic activity and Signaling



Introduction

Atrophy has been reported in multiple brain regions, even in the early stages of Parkinson’s disease.^{1–3} However, less is known about the progression of tissue loss after diagnosis.⁴ There have been a few studies of MRI-derived measures over time, but they were limited by small sample sizes,^{5,6} short follow-up durations^{7,8} or use of global volumetric measures.^{9–11} The most consistent findings are subcortical tissue loss early on, notably affecting striatum, thalamus, amygdala and hippocampus, and more widespread cortical atrophy when longer durations or larger sample sizes are used. With few exceptions,⁷ no study has

attempted to relate the spatial pattern of atrophy progression to intrinsic properties of the brain, such as anatomical connectivity, cellular composition or regional gene expression. Such an analysis could provide information about pathophysiological mechanisms in Parkinson’s disease.

There is increasing evidence that brain connectivity may shape tissue loss in a multitude of neurodegenerative and psychiatric diseases, including schizophrenia, frontotemporal dementia, amyotrophic lateral sclerosis, Alzheimer’s and Parkinson’s disease.^{7,12–18} This pattern points to the possibility of pathogenic agents spreading from neuron to neuron as a common mechanism. In Parkinson’s disease, converging evidence points to misfolded α -synuclein as the

propagating agent.^{19–24} Most α -synuclein aggregates are localized in synapses where they are thought to interfere with neurotransmitter release and cause dendritic spine loss^{2,5,26} that may be detectable using MRI-based measures, such as cortical thickness or deformation-based morphometry (DBM). Indeed, using a single time point or follow-up, we previously demonstrated that the MRI-derived baseline atrophy pattern and the atrophy progression after 1 year in *de novo* Parkinson's disease are consistent with a connectome-based propagation,^{2,7,16} a finding that has been replicated computationally in animal models.²⁴ However, the role of connectivity in explaining the longitudinal progression of atrophy in Parkinson's disease has not yet been tested in human patients followed longitudinally with multiple MRI time points.

The progression of brain atrophy is likely not only explained by brain connectivity but also by regional variations in tissue vulnerability.^{16,27} Indeed, some brain areas with higher α -synuclein concentration appear to be more susceptible to injury but also more likely to act as disease propagators.^{16,28,29} Regional vulnerability may additionally depend on the local cellular distribution or gene expression patterns that render the milieu to be more neurotoxic or neuroprotective.^{30–32} For instance, microglia have been implicated in both neuroprotection and neurotoxicity via regulation of inflammation.^{32,33} Astrocytes have been shown to accumulate α -synuclein and produce proinflammatory cytokines and chemokines.³¹ Oligodendrocytes may be targeted by neurodegeneration but can also play a role in neuroprotection via the synthesis of neurotrophic factors.³⁴ Endothelial cells have also been implicated in the progression of neural damage in Parkinson's disease³⁵ and blood–brain barrier (BBB) dysfunction is thought to play a role in the pathology associated with Parkinson's disease and other neurodegenerative diseases.^{36,37} On the other hand, endothelial cells have also been shown to contribute to neuron survival under certain physiological and inflammatory conditions.^{38,39} Finally, the ratio of excitatory to inhibitory neurons could be relevant for disease pathology, as excitotoxicity has also been implicated in Parkinson's disease, possibly in synergy with glial dysfunction.⁴⁰ A virtual histology approach may help explain how cellular composition relates to local vulnerability to atrophy.⁴¹

How brain architecture, local cell-type distribution and gene expression combine to determine the pattern of disease progression remains unknown. Here, we first mapped the progression of brain atrophy using DBM and then related it to structural and functional networks, cell-type composition and gene ontology (GO) enrichment analyses. We hypothesized that the constraints imposed by structural and functional networks as well as the regional differences in cell-type composition would jointly shape the pattern of atrophy found in Parkinson's disease. We show that the brain's connectome significantly shapes the course of atrophy over 4 years and that oligodendrocytes and endothelial cells may play a role in

neuroprotection, while GO analysis points to synapses as an important target of neurodegeneration.

Materials and methods

Data acquisition

All clinical and structural MRI data were downloaded in July 2019 from the Parkinson's progression markers initiative (PPMI, <http://www.ppmi-info.org>), a longitudinal multi-centre database including *de novo* Parkinson's disease participants and healthy controls (HCs).⁴² Clinical measures and T₁-weighted MRI acquired on 3 and 1.5 T scanners at baseline, 1, 2 and 4 years were used in this study (see Table 1). Acquisition parameters and detailed protocols are described on the PPMI website (https://www.ppmi-info.org/sites/default/files/docs/PA2_PPMI_Clinical%20Protocol_Final_01Feb2021.pdf Last accessed, March 2021). For each analysis, participants with missing data at one or more time points were excluded. Each participating centre received approval from a local research ethics committee. All the procedures and tests followed these committees' guidelines. Informed consent was obtained from each participant according to the Declaration of Helsinki before the beginning of the study.

Participants

Table 1 describes the clinical characteristics of the participants with Parkinson's disease included in the present study at each time point (i.e. baseline, 1, 2 and 4 years). Participants met the inclusion criteria for PPMI (<http://www.ppmi-info.org/study-design/>, Last accessed, February 2021) described in the Supplementary material (p. 1). Participants with a history of Parkinson's disease medication use, including L-Dopa, dopamine agonists, monoamine oxidase B inhibitors or amantadine, within 60 days of the baseline visit, or with a diagnosis of dementia⁴³ were excluded from the study. HC participants in the PPMI database were aged ≥ 30 years old at the screening visit with no current neurological disorder. Exclusion criteria for HC were a Montreal Cognitive Assessment (MoCA) score ≤ 26 or a first-degree relative with idiopathic Parkinson's disease. There were a total of 403 patients with Parkinson's disease and 184 HCs with a T₁-weighted MRI at baseline. After visual inspection to exclude images with abnormalities, 74 patients (50 men and 24 women) had both MRI and clinical evaluation at each of the three follow-up time points and 157 HCs (115 men and 42 women) at baseline. Most exclusions were due to missing assessments at one of the time points. In addition, neuroimaging data passing quality control were available for 120 Parkinson's disease participants at baseline and 1 year and 109 at 2 years, and these were used to confirm our findings with larger sample sizes. We ensured that the control group was similar to the Parkinson's disease group

Table 1 Descriptive statistics for the 74 *de novo* Parkinson's disease patients included in this study

Characteristics	Baseline Mean (SD)	Year 1 Mean (SD)	Year 2	Year 4	F-test P-value	BI-1Y P-adjusted ^a	BI-2Y P-adjusted ^a	BI-4Y P- adjusted ^a
Gender (men/women)	50/24	50/24	50/24	50/24	NA	NA	NA	NA
Number of patients taking PD medication	0	55	66	71	NA	NA	NA	NA
Age (years)	60.2 (9.4)	61.2 (9.4)	62.3 (9.5)	64.3 (9.5)	NA	NA	NA	NA
Education (years)	15.2 (2.6)	NA	NA	NA	NA	NA	NA	NA
Disease duration (days)	221.9 (228.7)	602.4 (231.6)	967.3 (228.9)	1699.5 (234.4)	NA	NA	NA	NA
Motor features								
Hoehn and Yahr stage	1.46 (0.50)	1.64 (0.51)	1.73 (0.53)	1.78 (0.50)	<0.00005	0.01	0.001	<0.00005
MDS-UPDRS-III (total tremor)	3.62 (3.02)	4.06 (2.87)	4.45 (3.55)	4.68 (4.04)	0.02	0.81	0.12	0.09
MDS-UPDRS-III (total rigidity)	3.64 (2.67)	4.43 (2.88)	4.91 (2.86)	5.43 (2.86)	<0.00005	0.02	<0.00005	<0.00005
MDS-UPDRS-III (total)	19.14 (8.53)	20.83 (10.08)	22.09 (11.32)	23.01 (9.40)	0.002	0.57	0.07	0.004
Non-motor features								
Epworth sleepiness scale score	4.19 (2.80)	4.16 (2.91)	4.55 (3.27)	4.67 (3.47)	0.23	NA	NA	NA
SCOPA-autonomic	8.58 (5.01)	10.13 (5.85)	10.91 (5.46)	11.94 (5.83)	<0.00005	0.02	<0.00005	<0.00005
Montreal Cognitive Assessment	27.40 (2.30)	27.04 (2.65)	26.78 (2.56)	27.28 (2.72)	0.12	NA	NA	NA
Phonemic Fluency (Letter F) ^b	12.33 (4.15)	13.97 (4.88)	14.07 (4.93)	14.87 (4.78)	<0.00005	0.045	0.02	<0.00005
Semantic Fluency Mean (fruit, animal, vegetables) ^b	16.45 (3.50)	16.36 (3.62)	16.86 (4.13)	16.98 (4.35)	0.24	NA	NA	NA
HVLT-Total Recall	25.32 (5.36)	24.71 (5.85)	24.43 (5.86)	24.07 (6.11)	0.14	NA	NA	NA
HVLT-Delayed Recall	8.56 (2.62)	8.69 (2.74)	8.65 (3.10)	8.28 (3.23)	0.5	NA	NA	NA
Letter-Number Sequencing	11.09 (2.75)	10.77 (2.55)	10.72 (2.98)	10.49 (3.43)	0.26	NA	NA	NA
Mood								
GDS-15 (Depressive symptoms)	1.99 (2.17)	2.07 (2.10)	2.32 (2.80)	2.26 (2.18)	0.64	NA	NA	NA
STAI (Anxiety)	93.59 (8.25)	91.96 (7.52)	91.68 (7.61)	92.99 (8.01)	0.22	NA	NA	NA
CSF biomarkers (pg/ml)								
Alpha synuclein (α -syn)	1455 (703)	1423 (666)	1412 (650)	NA	0.84	NA	NA	NA
Beta-amyloid (A β)	852 (354)	865 (366)	899 (354)	NA	0.28	NA	NA	NA
Phospho-tau (pTau)	13.27 (4.84)	13.24 (5.26)	13.44 (4.73)	NA	0.76	NA	NA	NA
Total Tau (tTau)	156 (52)	158 (59)	161 (51)	NA	0.51	NA	NA	NA
NFL	11.3 (6.3)	12.6 (7.3)	13.6 (7.5)	NA	0.001	0.002	0.001	NA

^aBonferroni correction.

^bNumber of words in one minute.

BI, baseline; 1Y, 1 year from baseline; 2Y, 2 years from baseline; 4Y, 4 years from baseline; CSF, cerebrospinal fluid; GDS: Geriatric Depression Scale; HVLT: Hopkins Verbal Learning Test; MDS-UPDRS, Movement Disorder Society Unified Parkinson Disease Rating Scale; SCOPA: SCAles for Outcomes in PArkinson's disease; SD, standard deviation; STAI: State-Trait Anxiety Inventory. Values in bold are significant at $p < 0.05$.

($n = 74$) relative to age at baseline (HC mean = 60.1 years, range: 31–83; Parkinson's disease patients mean = 60.2 years, range: 38–82 years; $P = 0.96$) and sex ($\chi^2 = 0.09$, $P = 0.77$).

We also assessed the sample for attrition bias, whereby more severely affected individuals tend to drop out of a longitudinal study. We used our previous classification of the patients in this dataset into three severity groups based on their baseline brain atrophy, which yielded mild, intermediate and severe subtypes.⁴⁴ The drop-out rates were 38, 39 and 58% for mild, intermediate and severe subtypes at 2 years ($\chi^2 = 5.8$, $P = 0.05$) and 60, 57, and 70% at 4 years ($\chi^2 = 2.5$, $P = 0.30$). This suggests that our dataset may have included less severely

affected participants (compared to the entire *de novo* sample), especially at the 2-year time point. Such a bias could obscure associations (e.g. between symptom severity and brain atrophy).⁴⁵

Brain structural analysis

Deformation-based morphometry

DBM quantifies voxel-wise brain tissue atrophy by performing non-linear transformations from the participant's brain to a template brain. DBM maps were derived from each participant's T₁-weighted MRI image at each time

point using the Computational Anatomy Toolbox (CAT12)⁴⁶ implemented in Statistical Parametric Mapping software (SPM12) (see [Supplementary material](#) for the detailed protocol, p. 2). The preprocessing and DBM calculation were performed separately for each T₁-weighted MRI image. Every voxel value represents the factor by which each voxel of the participant's brain has to expand (positive value) or shrink (negative value) to be registered to the MNI template.

W-score maps were generated to account for age and sex on brain deformation.^{47,48} A W-score map was computed for each time point (baseline, 1, 2 and 4 years) using the following formula, at each voxel:

$$W_i = \frac{DBM_i - DBM_{exp}}{\text{SD of residuals in controls}} \quad (1)$$

where W_i is the W-score at voxel i for a participant, DBM_i is the computed DBM value at voxel i , DBM_{exp} is the expected DBM value for that participant defined by $(\beta_1 * \text{age} + \beta_2 * \text{sex} + \beta_3)$, and derived from HC data. All statistical analyses involving DBM were performed using the W-scored DBM maps. Negative W-score values indicate atrophy (reduced volume) whereas positive W-scores indicate expansion, with normal ageing and sex effects accounted for. Only the baseline HC data were used as a reference since only a limited number of HC had longitudinal measurements.⁴⁹

Brain atrophy progression analysis

The pattern of atrophy progression was investigated voxel-wise using two SPM12 toolboxes: CAT12⁴⁶ and the probabilistic approach for threshold-free cluster enhancement (pTFCE),⁵⁰ written in MATLAB (R2018b). A two-tailed repeated measures ANOVA (F-contrast) with time as covariate followed by post hoc paired comparisons [t-contrasts between baseline (Bl) and 1 year, Bl and 2 years, Bl and 4 years] combined with the pTFCE based on Bayes' rule were used to compare atrophy differences between time points in the Parkinson's disease group. In all cases, W-score maps were used. Although sex was accounted for in the W-score calculation, we added it as a covariate in the repeated measures ANOVA to regress out its effect, as sex differences in atrophy were recently demonstrated in Parkinson's disease.⁴⁹ Scanner site was also added as a covariate. Family-wise error (FWE) rate (threshold: $P_{FWE} < 0.05$) was used to correct for multiple comparisons. Only significant clusters with 10 voxels or more were retained. This analysis was computed for the 74 participants with a T₁-MRI at each of the four time points. Additional analyses (t-contrasts between Bl and 1 year or Bl and 2 years) were done with all the patients who had a T₁-MRI at either baseline and 1 year ($N=120$) or baseline and 2 years ($N=109$). Afterwards, the Cammoun atlas⁵¹ was used to find the anatomical location of the significant clusters in the brain.

To understand how tissue changes relate to brain function, the mean atrophy progression was computed for each of the seven cortical resting-state networks defined by Yeo et al.⁵² These networks are thought to represent the distributed neural systems that support diverse cognitive domains.⁵³ One-sample permutation tests were computed to compare the mean atrophy progression of each network to its null distribution (two-sided P -value). Statistical significance was estimated by permutation testing using the netneurotools toolbox (<https://netneurotools.readthedocs.io/en/latest/index.html>, Last accessed, August 2021): network labels were permuted 1000 times while preserving the spatial autocorrelation, and network-specific means were recalculated to generate a null distribution for each network.^{54,55}

To investigate the relationship between atrophy progression and the synaptic organization and hierarchy of different zones of the cortex, the cortical regions were defined following the nomenclature of Mesulam.⁵⁶ The mean atrophy progression scores for each cortical tissue type (paralimbic, heteromodal, unimodal and idiosyncratic) were compared using a one-way ANOVA and *post hoc* tests with Bonferroni corrections.

Correlations were computed to investigate the relationship between clinical measures (motor and non-motor symptoms, mood and CSF biomarkers) and atrophy progression in the whole brain, in the significant clusters and in each of the seven resting-state networks (threshold: $P_{FDR} < 0.05$, two-tailed). Partial Spearman's correlations were used due to some data being non-normally distributed, with age, sex and education as covariates (only age and sex were used for motor symptoms).

Structural and functional network analysis

We next investigated the network spread hypothesis of Parkinson's disease. We tested whether the atrophy progression observed in each region was correlated with the atrophy progression of its structurally and functionally connected neighbourhood. In brief, (i) the brain was parcellated into equally sized cortical regions at four different spatial resolutions⁵¹; (ii) the mean atrophy progression was calculated for each region; (iii) matrices of structural and functional connectivity between regions were constructed, using diffusion-weighted MRI tractography and resting state functional MRI acquired on a different dataset of 70 healthy adults⁵⁷; (iv) the collective neighbourhood atrophy progression of each region was calculated, using the structural and functional networks to define the neighbours; (v) correlations were computed between the atrophy progression in each region and its collective neighbourhood atrophy progression; and (vi) the significance of the correlations was tested against a null model preserving spatial autocorrelation. (See the

detailed protocol in the [Supplementary material](#), p. 2–4.). This network analysis approach was previously used in schizophrenia.¹⁵

Complementary analysis on the role of functional connectivity

Additional analyses were performed to verify whether FC, without considering the structural connections between regions, is related to atrophy progression. Pearson's correlations were calculated between the regional atrophy progression and the collective deformation weighted by the FC of (i) the non-structurally connected direct neighbours (i.e. only region pairs not demonstrating structural connectivity, as defined above) and (ii) all the regions irrespective of their structural connections. These correlations were compared against spatial autocorrelation null models (1000 spins, two-tailed). The *cocor* package was used to statistically compare the magnitude of the correlations and calculate a Zou's confidence interval.⁵⁸

Cell-type analysis

Virtual histology

We next investigated if the atrophy progression was associated with the prevalence of specific cell types in the cortex, notably astrocytes, endothelial cells, microglia, excitatory and inhibitory neurons, oligodendrocytes and oligodendrocyte precursors. A virtual histology approach was used to correlate the neuroimaging data with cell-specific gene expression across brain regions.^{59,60} Every class of cell type was associated with a gene list first derived by Seidlitz et al.,⁴¹ from five single-cell RNA sequencing studies of post-mortem human cortical samples^{61–65} (for the detailed protocol, see Hansen et al.⁶⁶). To generate cortical maps for each cell type, the spatial expression patterns of these gene lists were derived from post-mortem brain data from six donors available in the Allen Human Brain Atlas (AHBA) genetics dataset.⁶⁷ Cell-type distribution was computed for each region of the Cammoun atlas⁵¹ at four different resolutions (68, 114, 219 and 448 cortical regions) using the abagen toolbox (<https://github.com/rmarkello/abagen>, Last accessed, August 2021) and the recommendations laid out by Arnatkeviciute et al.^{68,69} Pearson's correlations were calculated between the atrophy progression of each region and the region's average gene expression of each cell class. All the correlations were tested against null models preserving spatial autocorrelation (1000 spins; two-tailed).⁵⁵

Null model

The null models used in this study preserved the spatial autocorrelation between regions using the netneurotools toolbox.⁵⁵ This approach generates a null model by projecting the brain regions onto a sphere and randomly rotating the sphere (see Markello and Misic⁷⁰ for a comparison of different spatially constrained null models). Briefly, a surface-based representation of the different resolution parcellations of the Cammoun atlas on a FreeSurfer (release v6.0.0) surface was created. The spherical projection of the surface was then used to define spatial coordinates for each region by selecting the vertex closest to the center of mass of the region. The spatial coordinates were used to create null models by rotating and reassigning region values 1000 times. The spatial rotation was performed at the parcel resolution and in one hemisphere before being mirrored to the other. For the correlation analysis, the Pearson's correlation coefficients (observed values) were tested against the distributions of correlation coefficients derived from the null networks (permuted values).

GO enrichment analysis

A GO enrichment analysis was performed to explore the biological processes related to atrophy progression over 2 and 4 years using brain regional gene expression. To do this, we extracted the average gene expression value for all genes available in the AHBA genetics dataset (i.e. 15 633)⁶⁷ for each of the 448 cortical regions of the Cammoun atlas using the abagen toolbox and following previous recommendations.^{68,69} For investigating the functions of the genes associated with atrophy, we only selected the genes whose expression significantly correlated with atrophy progression after false discovery rate (FDR) correction and when compared to a null model preserving the spatial autocorrelation (1000 spins; two-tailed). This yielded lists of genes whose expression pattern was positively or negatively correlated with atrophy progression at 2 (positive correlation: $N=619$ genes, negative correlation: 1058 genes) and 4 years (positive correlation: $N=900$ genes, negative correlation: 1546 genes). We next investigated if the proportion of GO terms for the genes correlated to atrophy (i.e. the target gene list) significantly differed from the proportion of GO terms found with all genes extracted from the AHBA (i.e. background gene list). To ensure that the results were not due to the choice of a particular classification system, two publicly available GO platforms were used to obtain GO terms: the Gene Ontology enrichment analysis and visualization tool (GORilla)⁷¹ and the PANTHER Classification System.⁷² Of the 15 633 genes available in the AHBA genetics dataset, 13 992 and 14 657 genes were associated with a GO term in the GORilla (GO Process) and PANTHER (GO biological process) platforms, respectively. Supported gene IDs are

available from the GOrilla (<http://cbl-gorilla.cs.technion.ac.il>, Last accessed, February 2021) and PANTHER (www.pantherdb.org, Last accessed, February 2021) websites. For both platforms, a statistical overrepresentation analysis was conducted with Bonferroni correction to control for multiple comparisons. Whereas a hypergeometric model was implemented in GOrilla, the Fisher's exact test was used in PANTHER.

Data availability

MRI data used in this article are available for download at www.ppmi-info.org/data. All other datasets and software used are available from the sources cited in the Methods. The DBM atrophy progression maps will be made available on request.

Results

Clinical measures and CSF biomarkers

For each feature and CSF biomarker presented in Table 1, two-tailed repeated measures ANOVA with *post hoc* comparisons and Bonferroni–Holm correction⁷³ were used to evaluate the progression after 1, 2 and 4 years. All measures of motor severity worsened over time, namely Hoehn and Yahr stage ($P < 0.00005$), total UPDRS-III ($P = 0.002$), tremor ($P = 0.02$) and rigidity ($P < 0.00005$). At each follow-up, the Hoehn and Yahr stage and total rigidity score were significantly different from baseline while the total UPDRS-III showed a significant difference only after 4 years (P -adjusted = 0.004). Of the non-motor measures, only the Scale for outcomes in PD (SCOPA)-autonomic and phonemic fluency scores (Letter F from MoCA) showed a significant difference with time (P -adjusted < 0.00005). Both scores were significantly different from baseline at each follow-up. While the autonomic score worsened with time, an improvement was observed in phonemic fluency possibly reflecting a medication and/or learning effect (note that participants were not on anti-parkinsonian medications at baseline). Among the CSF biomarkers, only the neurofilament light polypeptide, a possible biomarker of neurodegeneration,^{74,75} presented a significant increase with time ($P = 0.0001$), more specifically after 1 (P -adjusted = 0.002) and 2 years (P -adjusted = 0.001).

Brain atrophy

The DBM W-Score maps were used to analyse voxel-wise atrophy progression after 1, 2 and 4 years in the participants with Parkinson's disease. This analysis showed an effect of time (F-contrast, two-tailed) in 24 clusters. The Cammoun atlas⁵¹ was used to localize the significant clusters (Supplementary Tables 1–3), which were widely

distributed throughout the brain. Atrophy progression was mostly found in the caudate, nucleus accumbens, hippocampus, amygdala and the temporal, parietal, occipital and cingulate cortex.

Post hoc analysis

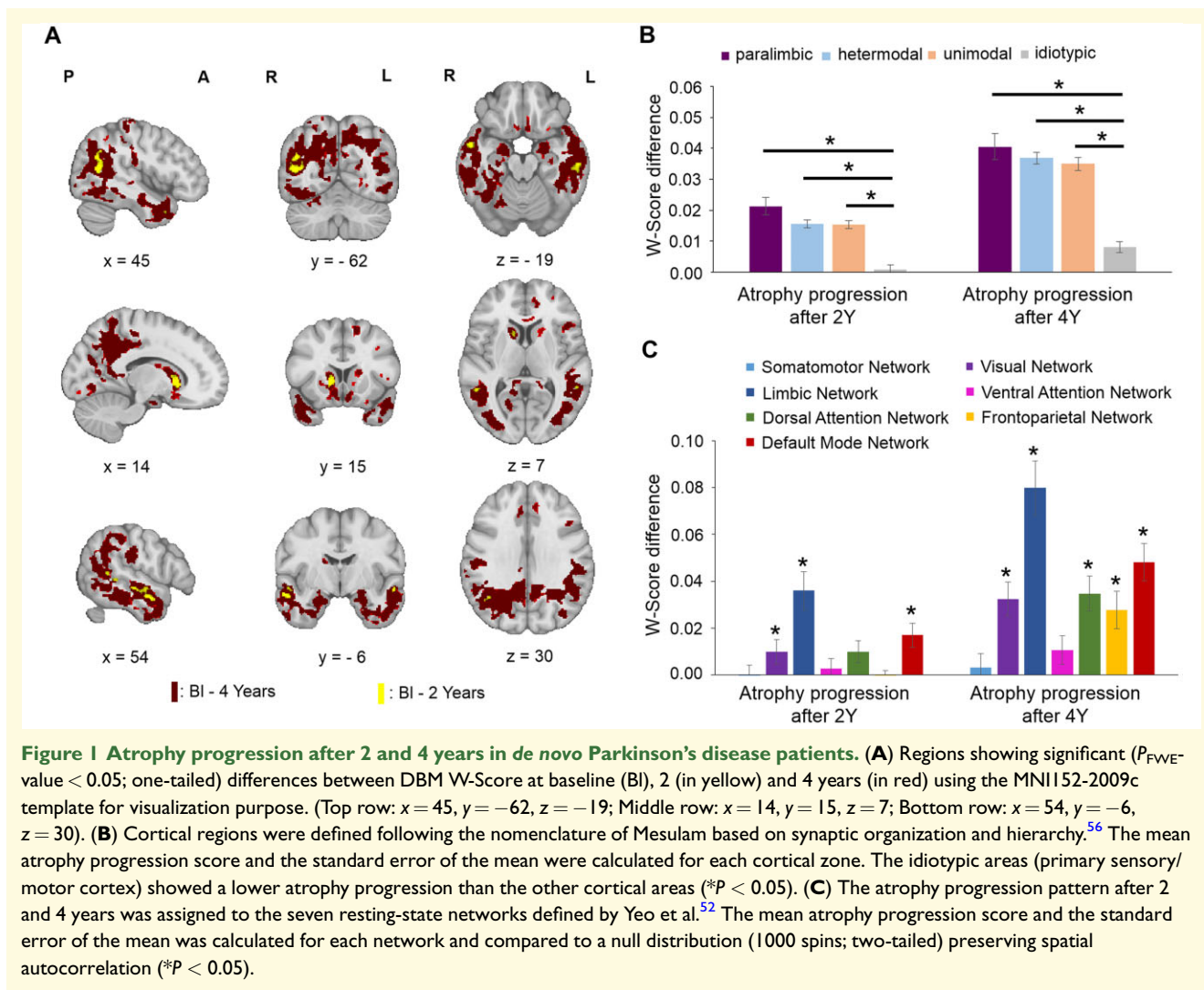
Post hoc tests (t-contrasts, one-tailed) were also computed between baseline and the three follow-up time points. Figure 1A shows the regions with a significant atrophy progression after 2 and 4 years. No significant clusters presented significantly greater atrophy after 1 year. After 2 years, 11 clusters were significant (Supplementary Table 2), located in the bilateral temporal lobe, left pre-cuneus, right caudate and angular gyrus. After 4 years, significant atrophy progression was found in 13 clusters (Supplementary Table 2), located in the right caudate, bilateral nucleus accumbens and temporal, parietal, occipital and cingulate cortex. Small clusters in the superior and inferior frontal gyrus were also found.

The previous results were derived from the participants who had scanning sessions at all time points. We repeated the 1- and 2-year analyses using the larger sample sizes of individuals who have not undergone scanning at all time points. A high overlap was observed between the regions with a significant atrophy progression at 2 years in the full 4-year sample (described above) and the regions with atrophy progression found after including participants with a T₁-MRI at baseline and 1 year ($N = 120$), or baseline and 2 years ($N = 109$) (Supplementary Fig. 1). Small clusters of atrophy progression were observed after 1 year in the additional analysis with 120 participants and larger clusters were found after 2 years with 109 participants (Supplementary Table 3).

Additional analysis, excluding subjects (HC and patients with Parkinson's disease) <50 years old was also performed to verify the impact of including younger subjects, but similar patterns of atrophy progression after 2 and 4 years were found (Supplementary Fig. 2).

To investigate the relationship with the synaptic hierarchy in the cortex, the average atrophy progression was compared between the paralimbic, heteromodal, unimodal and idiosyncratic cortical areas (Fig. 1B) as defined by Mesulam.⁵⁶ There was a significant effect of cortex type for the atrophy progression after 2 [$F(3,995) = 27.52$, $P < 0.00005$] and 4 years [$F(3,995) = 36.42$, $P < 0.00005$]. *Post hoc* comparisons indicated that this was due to significantly less atrophy progression in idiosyncratic (primary sensory and motor) cortex than other types. The mean atrophy progression values of the idiosyncratic areas after both 2 ($M = 0.0009$, $SD = 0.02$) and 4 years ($M = 0.008$, $SD = 0.03$) were significantly lower compared to the atrophy progression in other areas ($P < 0.00005$).

To further localize the disease process, the average atrophy progression was computed for each of the seven resting-state networks defined by Yeo et al.⁵² and compared against a null distribution preserving the



spatial autocorrelation (1000 spins; two-tailed) (Fig. 1C). The mean atrophy progression was significant after 2 years in the limbic ($P_{spin} = 0.001$), default mode ($P_{spin} = 0.002$) and visual ($P_{spin} = 0.002$) networks. After 4 years, the mean atrophy progression was also significant in the dorsal attention ($P_{spin} = 0.001$), frontoparietal ($P_{spin} = 0.001$), limbic ($P_{spin} = 0.001$), default mode ($P_{spin} = 0.001$) and visual ($P_{spin} = 0.001$) networks. Only the somatomotor ($P_{spin} = 0.42$) and ventral attention ($P_{spin} = 0.10$) networks did not present a significant atrophy progression after 4 years. Overall, the limbic and default mode networks were most affected.

Relationship with clinical measures and CSF biomarkers

Correlation analyses were performed to investigate how the mean atrophy progression after 2 and 4 years related to 10 clinical characteristics [MDS-UPDRS-III (total), the non-motor features and depressive symptoms]

and all the CSF biomarkers presented in Table 1. Additional correlations with the different clusters of significant atrophy progression after 2 and 4 years were also computed (Supplementary Tables 4–6). Partial Spearman's correlations controlling for the effect of age, sex, and education were not significant before ($P < 0.01$; two-tailed) or after FDR corrections ($P_{FDR} < 0.05$; two-tailed). When investigating the association between the mean atrophy progression of the seven resting-state networks after 2 and 4 years and the change in clinical measures over the same time period, no significant correlations were found after correcting for multiple comparisons.

The influence of structural and functional connectivity

We next investigated if there was a network-specific distribution of atrophy progression. If this is the case, brain regions structurally and/or functionally connected with

neighbours showing more atrophy progression should also present more atrophy progression after 2 or 4 years. For both structural and functional connectivity, significant correlations against spatial null models were found between the atrophy progression of a region and the atrophy progression of its connected neighbours after 2 years (structural: $r=0.61$, $P\text{-value}_{\text{spin}}=0.0001$; FC: $r=0.62$, $P\text{-value}_{\text{spin}}=0.0001$; two-tailed) and 4 years (structural: $r=0.61$, $P\text{-value}_{\text{spin}}=0.0001$; FC: $r=0.64$, $P\text{-value}_{\text{spin}}=0.0001$; two-tailed) at a parcellation of 448 cortical regions (Fig. 2). The results were replicated at all other spatial resolutions (Supplementary Fig. 3).

FC from resting state fMRI is constrained by structural connectivity.⁷⁶ To verify more specifically its influence on atrophy progression, we investigated the relationships between the regional atrophy progression and the collective deformation weighted by the FC of (i) the non-structurally connected neighbours and (ii) all the regions irrespective of their structural connections. Table 2 shows that, in both cases, correlations were markedly reduced. These results were replicated at the other spatial resolutions. Altogether, this finding suggests that both structural and functional connectivity are associated with atrophy

progression, but that neuronal activity modulates co-atrophy between structurally connected regions.

Relationship with cell-type distribution

In addition to connectivity, local factors may also influence atrophy progression in Parkinson's disease. Here, we investigated the relationship between the relative regional prevalence of different cell types and cortical atrophy progression. Two cell types were associated with relatively less atrophy progression. Using the Cammoun atlas with 448 regions, significant negative correlations were found between the prevalence of endothelial cells and atrophy progression after 2 ($r=-0.15$, $P\text{-value}_{\text{spin}}=0.04$, two-tailed) and 4 years ($r=-0.19$, $P\text{-value}_{\text{spin}}=0.01$, two-tailed) (Fig. 3). The atrophy progression was also inversely correlated with the prevalence of oligodendrocytes after 2 ($r=-0.11$, $P\text{-value}_{\text{spin}}=0.049$, two-tailed) and 4 years ($r=-0.11$, $P\text{-value}_{\text{spin}}=0.04$, two-tailed). In addition, negative correlations were obtained with three lower resolutions [68, 114 and 219 regions (R)] (see Supplementary Fig. 4). Only the correlations between the atrophy

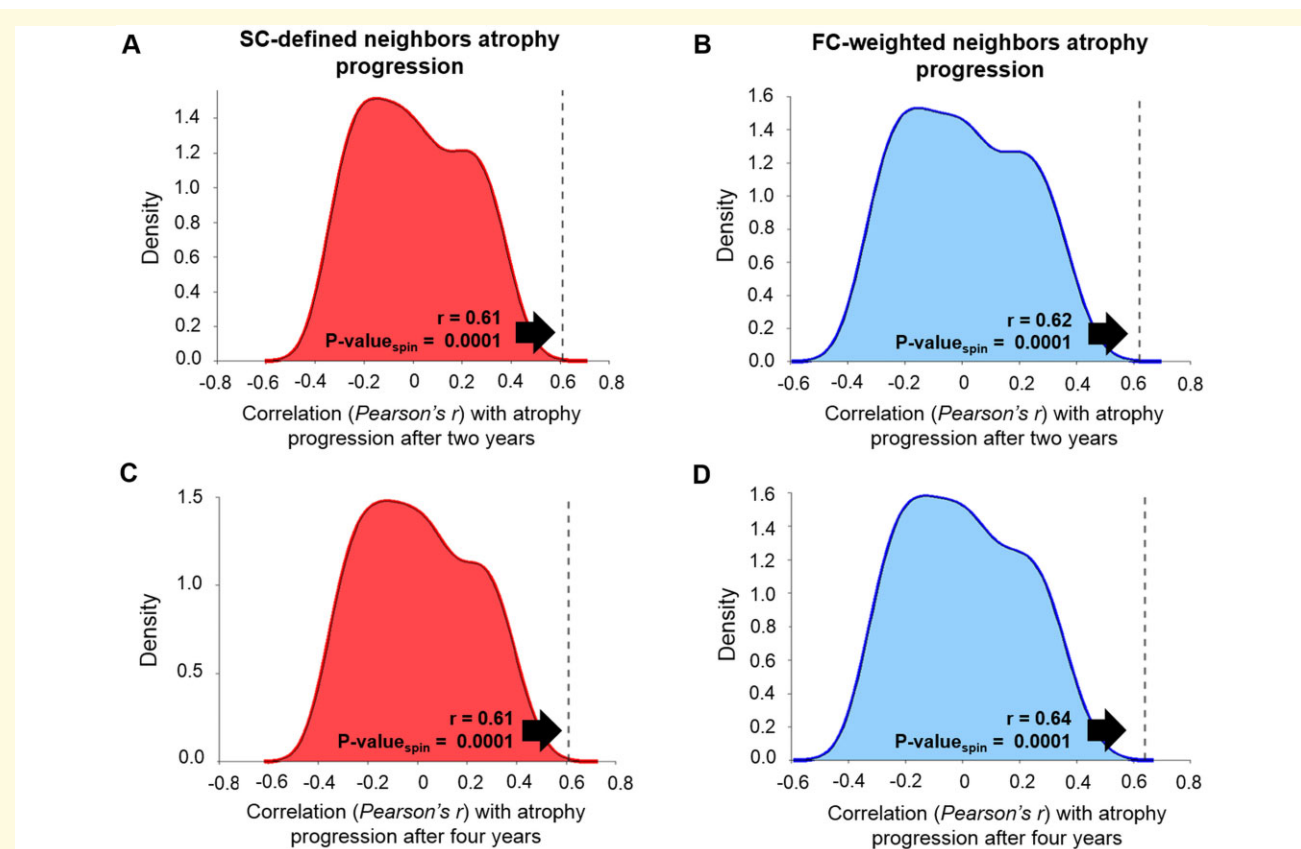
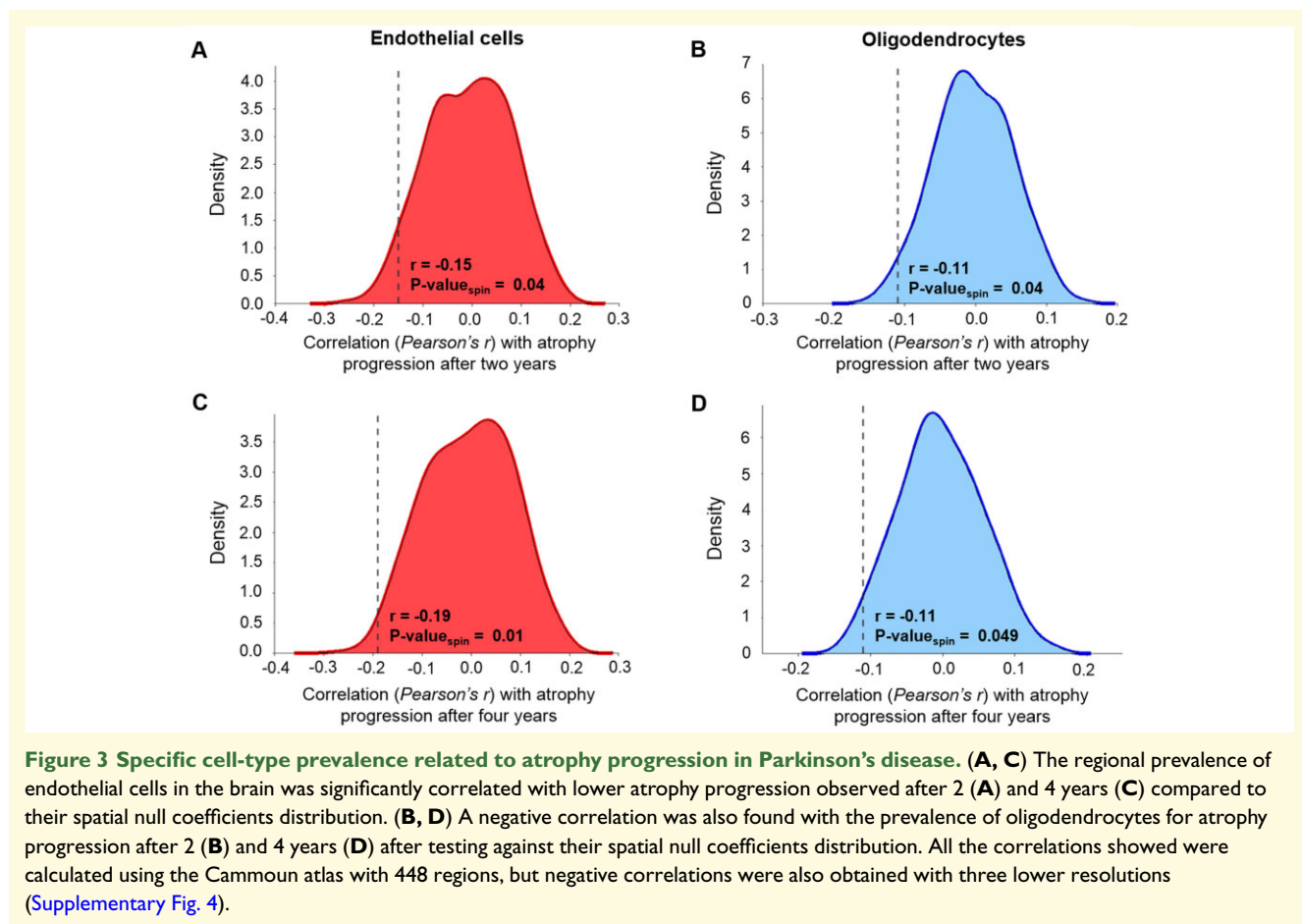


Figure 2 Atrophy progression relationship with structural and functional connectivity. (A, C) Regional atrophy progression was significantly correlated with the atrophy progression of the structurally connected (SC) neighbouring regions after 2 (A) and 4 years (C) compared to their spatial null coefficients distribution. (B, D) Regional atrophy progression was also related to the atrophy progression of the neighbouring regions weighted by their FC after 2 (B) and 4 years (D). These correlations were also tested against a null coefficients distribution using a model preserving the spatial autocorrelation between regions. All the correlations showed were calculated using the Cammoun atlas with 448 regions, but similar results were obtained with three other resolutions (Supplementary Fig. 3).

Table 2 Influence of functional connectivity on atrophy progression

Resolution	Structurally connected neighbours		Non-structurally connected neighbours		All regions		Comparisons			
	Correlation between regions and neighbors' atrophy progression (FC-weighted)		Correlation between regions and neighbors' atrophy progression (FC-weighted)		Correlation between all regions atrophy progression (FC-weighted irrespective of their structural connections)		Correlation with structurally vs. non-structurally connected neighbors		Correlation with structurally connected neighbors vs. all regions	
	Pearson's r	P -value spin test	Pearson's r	P -value spin test	Pearson's r	P -value spin test	Zou's 95% CI			
After 2 years										
68	0.66	0.008	0.25	0.14	0.45	0.08	0.16–0.66		0.04–0.40	
114	0.66	0.0009	0.27	0.08	0.49	0.006	0.22–0.57		0.06–0.29	
219	0.64	0.0004	0.34	0.03	0.49	0.001	0.19–0.41		0.08–0.23	
448	0.62	0.0001	0.33	0.04	0.43	0.0008	0.22–0.36		0.13–0.25	
After 4 years										
68	0.70	0.001	0.46	0.003	0.59	0.002	0.03–0.46		–0.05 to 0.29	
114	0.65	0.0007	0.42	0.002	0.56	0.0007	0.08–0.39		–0.02 to 0.21	
219	0.65	0.0003	0.39	0.009	0.50	0.0009	0.16–0.37		0.07–0.24	
448	0.64	0.0001	0.33	0.03	0.42	0.002	0.24–0.39		0.16–0.28	



progression after 4 years and the endothelial cells were significant at the three other resolutions (68R: $r = -0.33$, $P\text{-value}_{\text{spin}} = 0.04$; 114R: $r = -0.33$, $P\text{-value}_{\text{spin}} = 0.003$; 219R: $r = -0.25$; $P\text{-value}_{\text{spin}} = 0.049$) while the correlations between the atrophy progression after 4 years and oligodendrocytes were near statistical significance (68R: $r = -0.23$; $P\text{-value}_{\text{spin}} = 0.06$; 219R: $r = -0.14$; $P\text{-value}_{\text{spin}} = 0.06$) or significant (114R: $r = -0.21$; $P\text{-value}_{\text{spin}} = 0.049$). No significant correlation was found for the other five cell types (astrocytes, microglia, excitatory and inhibitory neurons and oligodendrocyte precursors) (Supplementary Fig. 5), and no cell type was associated with greater progression. These results seem to indicate slower cortical atrophy progression in regions with a higher prevalence of endothelial cells or oligodendrocytes.

Relationship with specific biological processes

To determine the functions of the genes whose expression was spatially associated with atrophy progression, a GO enrichment analysis was done. Two platforms, Gorilla and PANTHER, were used. The results from each platform consistently implicated terms related to synaptic function. Figure 4 shows the significant GO terms ($P\text{-value}_{\text{Bonferroni}} < 0.05$, two-tailed) from the genes positively associated with the atrophy progression after 2 ($N = 23$) and 4 years ($N = 17$), and their average fold enrichment. Individual platform results are shown in Supplementary Figs 6 and 7. The GO enrichment analysis revealed processes related to synaptic activity (regulation of synaptic plasticity Fig. 4A and B, fold enrichment = 3.61 and 3.33), chemical synaptic transmission (Fig. 4A and B, fold enrichment = 3.16 and 2.67) and cell signalling, namely trans-synaptic signalling (Fig. 4A and B, fold enrichment = 3.12 and 2.62), and cell-cell signalling (Fig. 4A and B, fold enrichment = 2.21 and 2.05) from the genes related to the atrophy progression after 2 (13 GO terms) and 4 years (10 GO terms). In sum, the GO analysis revealed that the regions showing greater atrophy progression tend to have greater expression of genes implicated in synaptic activity and cell signalling.

Additional analysis shows that 33 genes uncovered in this analysis were located in known Parkinson's disease GWAS loci⁷⁷ (Supplementary Tables 7 and 8), but future studies would be needed to examine whether these specific genes are driving the associations of the relevant loci with Parkinson's disease atrophy.

Discussion

Progressive brain atrophy was observed after 2 and 4 years in *de novo* Parkinson's disease after regressing out the effects of sex and normal ageing. The atrophy distribution was widespread, affecting five of the seven canonical resting-states networks⁵² at 4 years. In line with the

Braak hypothesis,¹⁹ cortical atrophy progression was determined by brain connectivity, supporting trans-neuronal propagation of the pathogenic process. Atrophy was greater in regions enriched for genes related to synaptic activity and signalling. In addition, cortical regions containing relatively more oligodendrocytes and endothelial cells had reduced vulnerability to atrophy. These findings may point to the biological mechanisms at play in neurodegeneration in Parkinson's disease. More generally, they support a model according to which neurodegeneration results from the interaction of a propagating agent with regional vulnerability.

Brain atrophy progression

Evaluating the progression of atrophy in the whole brain using DBM measures, we found small regions over the temporal and parietal lobe in addition to the right caudate nucleus presenting an atrophy progression after 2 years, while a more widespread atrophy progression in the caudate nucleus, nucleus accumbens and the temporal, parietal, occipital and cingulate cortex was observed after 4 years. This mostly posterior cortical pattern of atrophy progression is similar to the atrophy distribution observed in the ENIGMA-Parkinson's Study including 2367 patients with Parkinson's disease and 1183 HC.⁷⁸ Our findings showed alterations in the default mode, limbic, dorsal attention, frontoparietal and visual networks over this time. No relationship was found between the atrophy progression in any of the resting-state networks and the change in clinical symptoms. One explanation may be that the clinical measures available did not specifically target the regions showing atrophy progression. Indeed, motor deficits are mainly due to dopamine deficiency in the substantia nigra,⁷⁹ while autonomic dysfunction is mostly associated with brainstem and spinal neuronal loss in Parkinson's disease.⁸⁰ The substantia nigra may not show atrophy progression due to a floor effect (cell loss being already severe at presentation), while the brainstem is difficult to assess with DBM. Cortical atrophy patterns may be expected to relate to cognitive impairment; however, no cognitive decline was observed in this patient group, possibly due to a form of attrition bias affecting the PPMI cohort, whereby more severely affected individuals tended not to undergo the later MRI sessions. This may also explain why atrophy did not impinge on frontal areas in this sample. It is expected that more broadly distributed atrophy progression in later stages of the disease will eventually lead to cognitive deficits.⁸¹

Structural and functional connectivity mediates atrophy progression

We have previously shown that atrophy in *de novo* Parkinson's disease targets an intrinsic brain network,²

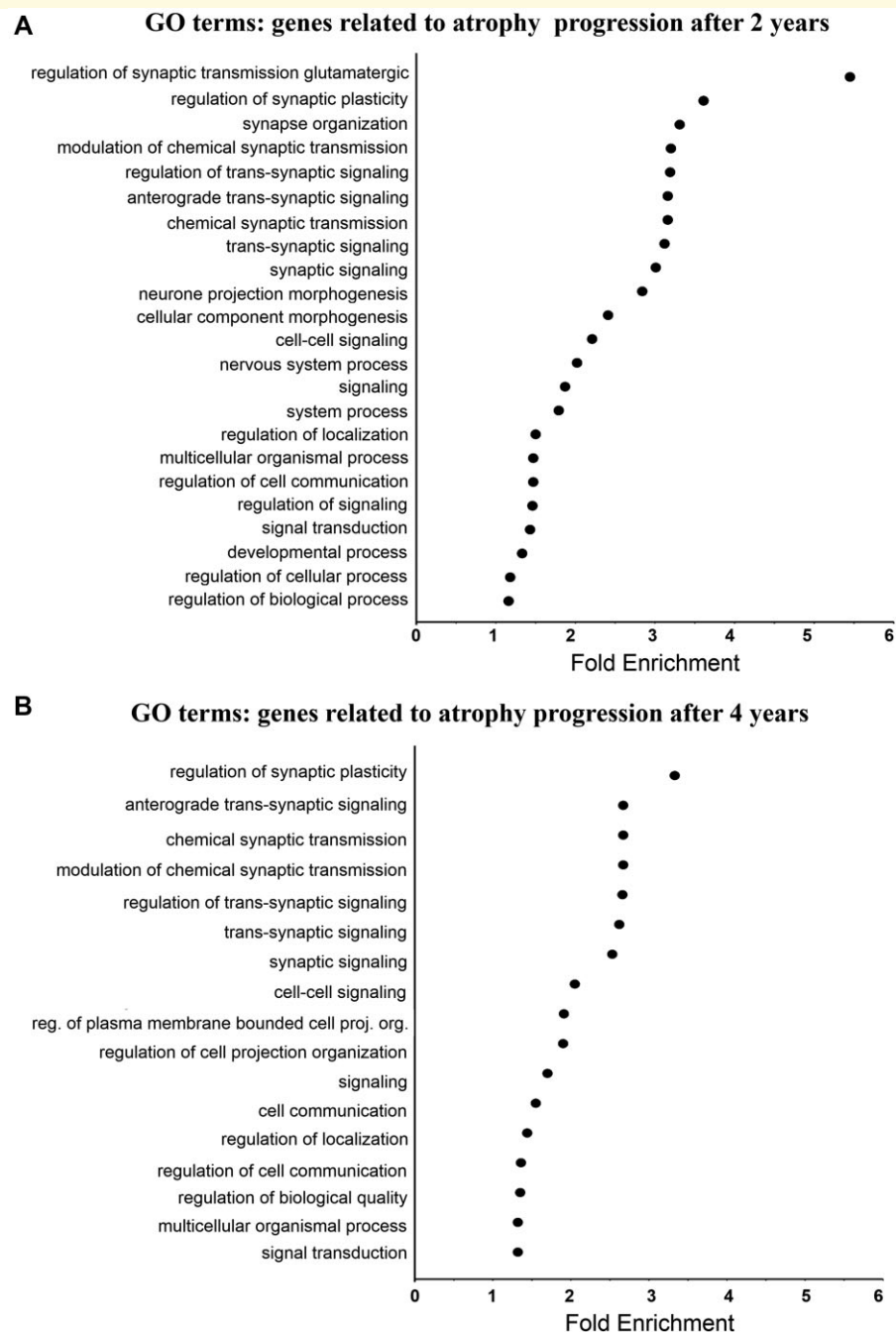


Figure 4 GO enrichment analysis of the genes related to atrophy progression in Parkinson's disease. The fold enrichment was obtained by calculating the ratio of the genes positively related to atrophy progression after 2 (A) and 4 years (B) over the number of expected genes for each GO term, based on the background genes list. Only the significant results ($P\text{-value}_{\text{Bonferroni}} < 0.05$) obtained with both platforms (GORilla and PANTHER) are shown here. The average fold enrichment values are the average from the two platforms. There was no significant GO term for the genes negatively associated with atrophy progression at both time points with either platform.

supporting the network spread hypothesis. Here, atrophy progression significantly affected five of the seven resting-state networks; however to test the role of connectivity, we asked whether cortical regions with greater atrophy progression were more likely to be structurally and functionally connected with each other. Correlations were

computed against spatial null models to control for the intrinsic relationships between proximal cortical regions. Our results indicate that both structural and functional connectivity are related to the atrophy progression after 2 and 4 years, even after controlling for regional autocorrelation in the brain. This is in line with studies

suggesting that atrophy in Parkinson's disease progresses via neuronal connectivity,^{2,7,14,16,21} most likely reflecting the spread of misfolded α -synuclein via neuronal projections.^{19,22,23,82} Moreover, our findings are in accordance with previous work showing that the atrophy pattern in other neurodegenerative diseases follows structural and functional brain network architecture.^{12,15,23,83}

Our previous work with an agent-based spreading model demonstrated that the pattern of brain atrophy depends on both neuronal connectivity and regional factors.¹⁶ Local vulnerability to neurodegeneration could depend on several factors including the prevalence of specific cell types.^{30–32} We next used gene-expression data to test for these local factors.

Cellular composition may reflect regional vulnerability

Using gene expression associated with different cell types in the healthy brain,⁴¹ the relationships between the prevalence of seven cell types (astrocytes, endothelial cells, microglia, excitatory and inhibitory neurons, oligodendrocytes and oligodendrocyte precursors) and atrophy progression were investigated. Only significant negative correlations were observed between regional atrophy progression and the prevalence of oligodendrocytes and endothelial cells in the cortex, suggesting a possible neuroprotective effect of both of these cell types. Our finding is in line with studies showing that oligodendrocytes promote neuronal survival by secreting trophic factors, such as brain-derived neurotrophic factor (BDNF), enhancing neuronal survival and axon regeneration, insulin-like growth factor 1 (IGF1), increasing the survival of young and aged cortical neurons and glial cell line-derived neurotrophic factor (GDNF), known for its neuroprotective effect on dopaminergic neurons.^{84–88} However, little is known about the role of oligodendrocytes in Parkinson's disease. A small number of α -synuclein inclusions has been observed in non-myelinating oligodendrocytes that may eventually contribute to neuronal death,³¹ but the production of neurotrophic factors by both myelinating and non-myelinating oligodendrocytes may override this neurotoxic effect. Oligodendrocyte genes have also been related to cortical synaptic density and likely play a role in synaptic elimination and maturation.⁸⁹

The role of endothelial cells and the BBB in the progression of Parkinson's disease is unclear. Some studies suggest that BBB alterations could contribute to neuropathological damage^{36,37} while others showed that endothelial cells contribute to neuronal survival under both physiological and inflammatory conditions.^{38,39} Endothelial cells are part of a neurovascular niche that supports neurogenesis in the adult brain.^{90–92} In addition, many angioneurins (including BDNF, IGF1 in addition to nerve, vascular endothelial, hepatocyte and epidermal growth factors) have receptors expressed by endothelial cells and have been shown to have

neuroprotective effects in different neurodegenerative disease models, including Parkinson's disease.⁹³ Angioneurins affect both neural and vascular cell function and regulate angiogenesis, BBB integrity, neuroregeneration, neuroprotection and synaptic plasticity.⁹³

Even though statistically significant, the correlations observed with both oligodendrocytes and endothelial cells were modest, indicating a need for further studies with animal models, larger samples of Parkinson's disease patients and later disease stages.

Regions prone to atrophy are enriched for synaptic genes

Regions with greater atrophy progression were enriched for genes implicated in synaptic plasticity, chemical synaptic transmission, trans-synaptic signalling and cell–cell signalling. This is consistent with post-mortem evidence that α -synuclein aggregates are mostly located in synapses.²⁵ Indeed, Lewy neurites, consisting of α -synuclein aggregates in presynaptic terminals, are a hallmark of Parkinson's disease pathology,⁹⁴ and one of the many functions of α -synuclein is to regulate synaptic homeostasis. Cell-culture experiments show that pathogenic α -synuclein fibrils first target pre-synaptic terminals and alter synaptic protein levels.⁹⁵ Thus, it is likely that misfolded α -synuclein first accumulates at synapses, causing impaired neurotransmission followed by synaptic and eventual axonal and neuronal death.²⁶ Pathological findings are mirrored by human imaging evidence showing that diffusion weighted MRI measures sensitive to neuritic damage are consistently abnormal in Parkinson's disease.^{49,96–98} Finally, synaptic and neuritic death should be associated with reduced neuropil and hence tissue loss, which should be reflected in the DBM measures used here.

It has also been demonstrated that α -synuclein can be transmitted from cell to cell in a prion-like manner.^{23,99} Two findings from our work support the α -synuclein synaptic dysfunction and synaptic spreading hypothesis: (i) the regions with greater atrophy progression were enriched for genes related to synaptic activity, cell–cell communication and signalling and (ii) atrophy was dependent on connectivity.

The link to synaptic proteins may also explain the relative distribution of tissue loss along the sensory-limbic cortical hierarchy. We found that primary sensory and motor cortical areas exhibited significantly less progressive atrophy than transmodal or paralimbic cortex, in keeping with Braak's observations.¹⁹ Primary areas have lower synaptic density,¹⁰⁰ but they also exist at the periphery of the brain connectome,⁵⁶ and are the most distant from limbic and default mode areas that appear to be affected early in the course of the disease. Thus, connectivity and local features may both account for the fact that primary areas are affected in the last stage of Parkinson's disease.

Strengths and limitations

Strengths of the study include the use of DBM, which allows the detection of both cortical and subcortical changes and has been shown to be more sensitive than VBM to subcortical volume loss in early Parkinson's disease.^{2,101} Secondly, the atrophy progression measure accounts for the expected effects of sex and normal ageing by using the W-score approach. Thirdly, using a longitudinal design with the same participants at all time points limits drop-out effects that may affect brain measures derived from a different number of participants at each time point.^{9,44,102} Given the well-known clinical heterogeneity in participants with Parkinson's disease,^{103–105} looking at the data from the same participants in a longitudinal study ensures greater consistency and reduces confounding factors. Fourthly, having multiple follow-up time points (1, 2 and 4 years) also gives a more precise estimate of the trajectory of atrophy progression through time.

Some limitations should also be acknowledged. Follow-up duration for the clinical and neuroimaging data is relatively short (4 years) and longer follow-up should help to determine the relationships between atrophy progression and cognitive dysfunction, mood symptoms and CSF biomarkers. Moreover, the PPMI database includes measures from multiple centres which may lead to site or scanner specific biases. However, PPMI has strict guidelines and protocols to acquire the clinical and imaging data to ensure standardization⁴² and scanner site was used as covariate in all our analyses. Also, we combined data acquired at two different MRI field strengths. But it is noteworthy that, in a previous study, the DBM pattern observed at baseline in PPMI using 3 T T₁weighted MRI was replicated at 1.5 T,² suggesting that the use of different magnetic field intensities in the current analysis (3 T and 1.5 T) did not impact our findings. In addition, only participants with Parkinson's disease with neuroimaging data at all four points were included in the main analysis, possibly excluding those with more severe symptoms and/or more atrophy (who are more predisposed to drop out of the study) and raising the possibility of survivor and collider bias.⁴⁵ The former could mask disease progression, while the latter could lead to biased estimates of associations. Note, however, that additional analyses were performed with larger sample sizes including participants with data at baseline and 1 year, and baseline and 2 years, and results were comparable. Also, since only a limited number of HC had longitudinal measurements, it was not possible to control for the intra-subject variability in normal ageing. Nevertheless, the normal ageing effect was regressed out at every time point using W-Scores. Finally, other structural neuroimaging measures (such as cortical thickness or diffusion-weighted MRI) should also be used to investigate the longitudinal progression of atrophy.

Conclusion

Widespread atrophy was found after 4 years in the early stages of Parkinson's disease. This pattern identified vulnerable brain regions that could eventually be used as a guide for other Parkinson's disease longitudinal studies. We also showed factors associated with disease progression, including connectivity and regional tissue composition. This may help identify biological processes implicated in the progression of Parkinson's disease. In addition, our results provide further support for the α -synuclein network spread hypothesis first proposed by Braak.

Supplementary material

Supplementary material is available at *Brain Communications* online.

Acknowledgements

The authors would like to thank Jakob Seidlitz for sharing his cell-type gene sets and for his valuable advice. We also thank Yashar Zeighami and Alexandre Hutton for their assistance. Data used in this article were obtained from the PPMI database (www.ppmi-info.org/data, Last accessed, July 2019). For up-to-date information on the study, visit: www.ppmi-info.org. PPMI—a public-private partnership—is funded by the Michael J. Fox Foundation for Parkinson's Research funding partners 4D Pharma, Abbvie, Acurex Therapeutics, Allergan, Amatus Therapeutics, ASAP, Avid Radiopharmaceuticals, Bial Biotech, Biogen, BioLegend, Bristol-Myers Squibb, Calico, Celgene, Dacapo Brain Science, Denali, The Edmond J. Safra Foundation, GE Healthcare, Genentech, GlaxoSmithKline, Golub Capital, Handl Therapeutics, Insite, Janssen Neuroscience, Lilly, Lundbeck, Merck, Meso Scale Discovery, Neurocrine Biosciences, Pfizer, Piramal, Prevail, Roche, Sanofi Genzyme, Servier, Takeda, Teva, UCB, Verily and Voyager Therapeutics.

Funding

This work was funded by grants from the Michael J Fox Foundation for Parkinson's Research, the Alzheimer's Association, the Weston Brain Institute, the Canadian Institutes of Health Research and the Healthy Brains for Healthy Lives (HBHL) initiative of McGill University. S.R. receives a scholarship from the Fonds de Recherche du Québec—Santé.

Competing interests

The authors report no competing interests.

References

- Mak E, Su L, Williams GB, et al. Baseline and longitudinal grey matter changes in newly diagnosed Parkinson's disease: ICICLE-PD study. *Brain*. 2015;138(Pt 10):2974–2986.
- Zeighami Y, Ulla M, Iturria-Medina Y, et al. Network structure of brain atrophy in de novo Parkinson's disease. *eLife*. 2015;4(e08440):1–20.
- Sterling N, Lewis M, Du G, Huang X. Structural imaging and Parkinson's disease: Moving toward quantitative markers of disease progression. *J Parkinsons Dis*. 2016;6(3):557–567.
- Sarasso E, Agosta F, Piramide N, Filippi M. Progression of grey and white matter brain damage in Parkinson's disease: A critical review of structural MRI literature. *J Neurol*. 2021;268(9):3144–3179.
- Ibarretxe-Bilbao N, Junque C, Segura B, et al. Progression of cortical thinning in early Parkinson's disease. *Mov Disord*. 2012;27(14):1746–1753.
- Tessa C, Lucetti C, Giannelli M, et al. Progression of brain atrophy in the early stages of Parkinson's disease: A longitudinal tensor-based morphometry study in de novo patients without cognitive impairment. *Hum Brain Mapp*. 2014;35(8):3932–3944.
- Yau Y, Zeighami Y, Baker T, et al. Network connectivity determines cortical thinning in early Parkinson's disease progression. *Nat Commun*. 2018;9(12):1–10.
- Sampedro F, Martínez-Horta S, Marín-Lahoz J, Pagonabarraga J, Kulisevsky J. Longitudinal intracortical diffusivity changes in de-novo Parkinson's disease: A promising imaging biomarker. *Parkinsonism Relat Disord*. 2019;68(September):22–25.
- Lewis MM, Du G, Lee EY, et al. The pattern of gray matter atrophy in Parkinson's disease differs in cortical and subcortical regions. *J Neurol*. 2016;263(1):68–75.
- Mollenhauer B, Zimmermann J, Sixel-Döring F, et al.; DeNoPa Study Group. Monitoring of 30 marker candidates in early Parkinson disease as progression markers. *Neurology*. 2016;87(2):168–177.
- Mak E, Su L, Williams GB, et al. Longitudinal whole-brain atrophy and ventricular enlargement in nondemented Parkinson's disease. *Neurobiol Aging*. 2017;55:78–90.
- Seeley WW, Crawford RK, Zhou J, Miller BL, Greicius MD. Neurodegenerative diseases target large-scale human brain networks. *Neuron*. 2009;62(1):42–52.
- Zhou J, Gennatas ED, Kramer JH, Miller BL, Seeley WW. Predicting regional neurodegeneration from the healthy brain functional connectome. *Neuron*. 2012;73(6):1216–1227.
- Pandya S, Zeighami Y, Freeze B, et al. Predictive model of spread of Parkinson's pathology using network diffusion. *Neuroimage*. 2019;192:178–194.
- Shafiei G, Markello RD, Makowski C, et al. Spatial patterning of tissue volume loss in schizophrenia reflects brain network architecture. *Biol Psychiatry*. 2020;87(8):727–729.
- Zheng YQ, Zhang Y, Yau Y, et al. Local vulnerability and global connectivity jointly shape neurodegenerative disease propagation. *PLoS Biol*. 2019;17(11):e3000495.
- Crossley NA, Mechelli A, Scott J, et al. The hubs of the human connectome are generally implicated in the anatomy of brain disorders. *Brain*. 2014;137(8):2382–2395.
- Meier JM, van der Burgh HK, Nitert AD, et al. Connectome-based propagation model in amyotrophic lateral sclerosis. *Ann Neurol*. 2020;87(5):725–738.
- Braak H, Del Tredici K, Rüb U, De Vos RA, Jansen Steur EN, Braak E. Staging of brain pathology related to sporadic Parkinson's disease. *Neurobiol Aging*. 2003;24(2):197–211.
- Braak H, Bohl JR, Müller CM, Rüb U, de Vos RA, Del Tredici K. Stanley Fahn lecture 2005: The staging procedure for the inclusion body pathology associated with sporadic Parkinson's disease reconsidered. *Mov Disord*. 2006;21(12):2042–2051.
- Brundin P, Melki R. Prying into the prion hypothesis for Parkinson's disease. *J Neurosci*. 2017;37(41):9808–9818.
- Jucker M, Walker LC. Propagation and spread of pathogenic protein assemblies in neurodegenerative diseases. *Nat Neurosci*. 2018;21(10):1341–1349.
- Luk K, Kehm V, Carroll J, et al. Pathological α -synuclein transmission initiates parkinson-like neurodegeneration in nontransgenic mice. *Science*. 2012;338(6109):949–954.
- Henderson MX, Cornblath EJ, Darwich A, et al. Spread of α -synuclein pathology through the brain connectome is modulated by selective vulnerability and predicted by network analysis. *Nat Neurosci*. 2019;22(8):1248–1257.
- Schulz-Schaeffer WJ. The synaptic pathology of α -synuclein aggregation in dementia with Lewy bodies, Parkinson's disease and Parkinson's disease dementia. *Acta Neuropathol*. 2010;120(2):131–143.
- Bellucci A, Mercuri NB, Venneri A, et al. Parkinson's disease: From synaptic loss to connectome dysfunction. *Neuropathol Appl Neurobiol*. 2016;42(1):77–94.
- Surmeier DJ, Obeso JA, Halliday GM. Parkinson's disease is not simply a prion disorder. *J Neurosci*. 2017;37(41):9799–9807.
- Freeze B, Acosta D, Pandya S, Zhao Y, Raj A. Regional expression of genes mediating trans-synaptic alpha-synuclein transfer predicts regional atrophy in Parkinson disease. *Neuroimage Clin*. 2018;18:456–466.
- Luna E, Decker SC, Riddle DM, et al. Differential α -synuclein expression contributes to selective vulnerability of hippocampal neuron subpopulations to fibril-induced toxicity. *Acta Neuropathol*. 2018;135(6):855–875.
- Teismann P, Schulz JB. Cellular pathology of Parkinson's disease: Astrocytes, microglia and inflammation. *Cell Tissue Res*. 2004;318(1):149–161.
- Halliday GM, Stevens CH. Glia: Initiators and progressors of pathology in Parkinson's disease. *Mov Disord*. 2011;26(1):6–17.
- Le W, Wu J, Tang Y. Protective microglia and their regulation in Parkinson's disease. *Front Mol Neurosci*. 2016;9:89.
- Block ML, Zecca L, Hong JS. Microglia-mediated neurotoxicity: Uncovering the molecular mechanisms. *Nat Rev Neurosci*. 2007;8(1):57–69.
- McTigue DM, Tripathi RB. The life, death, and replacement of oligodendrocytes in the adult CNS. *J Neurochem*. 2008;107(1):1–19.
- Cabezas R, Ávila M, Gonzalez J, et al. Astrocytic modulation of blood brain barrier: Perspectives on Parkinson's disease. *Front Cell Neurosci*. 2014;8:211.
- Stamatovic S, Keep R, Andjelkovic A. Brain endothelial cell-cell junctions: How to “open” the blood brain barrier. *Curr Neuropharmacol*. 2008;6(3):179–192.
- Luisant A, Artus C, Glacial F, Ganeshamoorthy K, Couraud P-O. Tight junctions at the blood brain barrier: Physiological architecture and disease-associated dysregulation. *Fluids Barriers CNS*. 2012;9(1):23.
- Bayas A, Hummel V, Kallmann B, Karch C, Toyka K, Rieckmann P. Human cerebral endothelial cells are a potential source for bioactive BDNF. *Cytokine*. 2002;19(2):55–58.
- Guo S, Kim WJ, Lok J, et al. Neuroprotection via matrix-trophic coupling between cerebral endothelial cells and neurons. *Proc Natl Acad Sci U S A*. 2008;105(21):7582–7587.
- Iovino L, Tremblay M, Civiero L. Glutamate-induced excitotoxicity in Parkinson's disease: The role of glial cells. *J Pharmacol Sci*. 2020;144(3):151–164.
- Seidlitz J, Nadig A, Liu S, et al. Transcriptomic and cellular decoding of regional brain vulnerability to neurodevelopmental disorders. *Nat Commun*. 2020;11(1):3358.
- Marek K, Jennings D, Lasch S, et al. The Parkinson Progression Marker Initiative (PPMI). *Prog Neurobiol*. 2011;95(4):629–635.
- Emre M, Aarsland D, Brown R, et al. Clinical diagnostic criteria for dementia associated with Parkinson's disease. *Mov Disord*. 2007;22(12):1689–1707.

44. Zeighami Y, Fereshtehnejad SM, Dadar M, et al. Assessment of a prognostic MRI biomarker in early de novo Parkinson's disease. *Neuroimage Clin.* 2019;24:101986.
45. Munafò MR, Tilling K, Taylor AE, Evans DM, Smith GD. Collider scope: When selection bias can substantially influence observed associations. *Int J Epidemiol.* 2018;47(1):226–235.
46. Gaser C, Dahnke R. CAT-A computational anatomy toolbox for the analysis of structural MRI data. *Hum Brain Mapp.* 2016; 32(7):336–348.
47. Boccardi M, Laakso MP, Bresciani L, et al. The MRI pattern of frontal and temporal brain atrophy in fronto-temporal dementia. *Neurobiol Aging.* 2003;24(1):95–103.
48. La Joie R, Perrotin A, Barre L, et al. Region-specific hierarchy between atrophy, hypometabolism, and b-amyloid (Ab) load in Alzheimer's disease dementia. *J Neurosci.* 2012;32(46): 16265–16273.
49. Tremblay C, Abbasi N, Zeighami Y, et al. Sex effects on brain structure in de novo Parkinson's disease: A multi-modal neuroimaging study. *Brain.* 2020;143(10):3052–3066.
50. Spisák T, Spisák Z, Zunhammer M, et al. Probabilistic TFCE: A generalized combination of cluster size and voxel intensity to increase statistical power. *Neuroimage.* 2019;185:12–26.
51. Cammoun L, Gigandet X, Meskaldji D, et al. Mapping the human connectome at multiple scales with diffusion spectrum MRI. *J Neurosci Methods.* 2012;203(2):386–397.
52. Yeo TB, Krienen FM, Sepulcre J, et al. The organization of the human cerebral cortex estimated by intrinsic functional connectivity. *J Neurophysiol.* 2011;106(3):1125–1165.
53. Petersen SE, Sporns O. Brain networks and cognitive architectures. *Neuron.* 2015;88(1):207–219.
54. Alexander-Bloch AF, Shou H, Liu S, et al. On testing for spatial correspondence between maps of human brain structure and function. *Neuroimage.* 2018;178:540–551.
55. Vázquez-Rodríguez B, Suárez LE, Markello RD, et al. Gradients of structure–function tethering across neocortex. *Proc Natl Acad Sci U S A.* 2019;116(42):21219–21227.
56. Mesulam MM. From sensation to cognition. *Brain.* 1998;121(6): 1013–1052.
57. Miić B, Betzel RF, Nematzadeh A, et al. Cooperative and competitive spreading dynamics on the human connectome. *Neuron.* 2015;86(6):1518–1529.
58. Diedenhofen B, Musch J. Cocor: A comprehensive solution for the statistical comparison of correlations. *PLoS One.* 2015;10(4): e0121945.
59. Shin J, French L, Xu T, et al. Cell-specific gene-expression profiles and cortical thickness in the human brain. *Cereb Cortex.* 2018;28(9):3267–3277.
60. Writing Committee for the Attention-Deficit/Hyperactivity Disorder, Autism Spectrum Disorder, Bipolar Disorder, et al. Virtual histology of cortical thickness and shared neurobiology in 6 psychiatric disorders. *JAMA Psychiatry.* 2020;78(1):47–63.
61. Darmanis S, Sloan SA, Zhang Y, et al. A survey of human brain transcriptome diversity at the single cell level. *Proc Natl Acad Sci U S A.* 2015;112(23):7285–7290.
62. Zhang Y, Sloan SA, Clarke LE, et al. Purification and characterization of progenitor and mature human astrocytes reveals transcriptional and functional differences with mouse. *Neuron.* 2016; 89(1):37–53.
63. Habib N, Avraham-Davidi I, Basu A, et al. Massively parallel single-nucleus RNA-seq with DroNc-seq. *Nat Methods.* 2017; 14(10):955–958.
64. Lake BB, Chen S, Sos BC, et al. Integrative single-cell analysis of transcriptional and epigenetic states in the human adult brain. *Nat Biotechnol.* 2018;36(1):70–80.
65. Li M, Santpere G, Kawasawa YI, et al.; BrainSpan Consortium. Integrative functional genomic analysis of human brain development and neuropsychiatric risks. *Science.* 2018;362(6420): 1444–1448.
66. Hansen J, Markello R, Vogel J, Seidlitz J, Bzdok D, Misić B. Molecular signatures of cognition and affect. *bioRxiv.* 2020; 2020.07.16.203026.
67. Hawrylycz MJ, Lein ES, Guillozet-Bongaarts A, et al. An anatomically comprehensive atlas of the adult human brain transcriptome. *Nature.* 2012;489(7416):391–399.
68. Arnatkeviciute A, Fulcher BD, Fornito A. A practical guide to linking brain-wide gene expression and neuroimaging data. *Neuroimage.* 2019;189:353–367.
69. Markello RD, Shafiei G, Zheng Y-Q, Misić B. abagen: A toolbox for the Allen Brain Atlas genetics data (0.1.3-doc). *Zenodo.* 2020. <https://doi.org/10.5281/zenodo.5129257>.
70. Markello RD, Misić B. Comparing spatial null models for brain maps. *Neuroimage.* 2021;236:118052.
71. Eden E, Navon R, Steinfeld I, Lipson D, Yakhini Z. GOrilla: A tool for discovery and visualization of enriched GO terms in ranked gene lists. *BMC Bioinformatics.* 2009;10:48.
72. Mi H, Muruganujan A, Casagrande JT, Thomas PD. Large-scale gene function analysis with PANTHER classification system. *Nat Protoc.* 2013;8(8):1551–1566.
73. Holm S. A simple sequentially rejective multiple test procedure. *Scand J Stat.* 1979;6(2):65–70.
74. Herrmann W, Obeid R. Biomarkers of neurodegenerative diseases. *Clin Chem Lab Med.* 2011;49(3):343–344.
75. Zetterberg H. Neurofilament light: A dynamic cross-disease fluid biomarker for neurodegeneration. *Neuron.* 2016;91(1):1–3.
76. Honey CJ, Sporns O, Cammoun L, et al. Predicting human resting-state functional connectivity from structural connectivity. *Proc Natl Acad Sci U S A.* 2009;106(6):2035–2040.
77. Grenn FP, Kim JJ, Makarious MB, et al.; the International Parkinson's Disease Genomics Consortium (IPDGC). The Parkinson's disease genome-wide association study locus browser GWS6 loci and gene selection. *Mov Disord.* 2020;35(11): 2056–2067.
78. Laansma MA, Bright JK, Al-Bachari S, et al. International Multicenter Analysis of Brain Structure Across Clinical Stages of Parkinson's Disease. *Movement Disorders : official Journal of the Movement Disorder Society.* 2021;36(11): 2583–2594.10.1002/mds.28706 34288137
79. Greffard S, Verny M, Bonnet AM, et al. Motor score of the unified Parkinson disease rating scale as a good predictor of lewy body-associated neuronal loss in the substantia nigra. *Arch Neurol.* 2006;63(4):584–588.
80. Metzger JM, Emborg ME. Autonomic dysfunction in Parkinson disease and animal models. *Clin Auton Res.* 2019;29(4): 397–414.
81. Ibarretxe-Bilbao N, Zarei M, Junque C, et al. Dysfunctions of cerebral networks precede recognition memory deficits in early Parkinson's disease. *Neuroimage.* 2011;57(2):589–597.
82. Masuda-Suzukake M, Nonaka T, Hosokawa M, et al. Prion-like spreading of pathological α -synuclein in brain. *Brain.* 2013; 136(Pt 4):1128–1138.
83. Cauda F, Nani A, Manuella J, et al. Brain structural alterations are distributed following functional, anatomic and genetic connectivity. *Brain.* 2018;141(11):3211–3232.
84. Dougherty K, Dreyfus C, Black I. Brain-derived neurotrophic factor in astrocytes, oligodendrocytes, and microglia/macrophages after spinal cord injury. *Neurobiol Dis.* 2000;7(6 Pt B):574–585.
85. Lin L-FH, Doherty DH, Lile JD, Bektesh S, Collins F. GDNF: A glial cell line - Derived neurotrophic factor for midbrain dopaminergic neurons. *Science.* 1993;260(5111):1130–1132.
86. Tomac A, Lindqvist E, Lin L, et al. Protection and repair of the nigrostriatal dopaminergic system by GDNF in vivo. *Nature.* 1995;373(6512):335–339.
87. Wilkins A, Chandran S, Compston A. A role for oligodendrocyte-derived IGF-1 in trophic support of cortical neurons. *Glia.* 2001;36(1):48–57.

88. Wilkins A, Majed H, Layfield R, Compston A, Chandran S. Oligodendrocytes promote neuronal survival and axonal length by distinct intracellular mechanisms: A novel role for oligodendrocyte-derived glial cell line-derived neurotrophic factor. *J Neurosci*. 2003;23(12):4967–4974.
89. Goyal MS, Raichle ME. Gene expression-based modeling of human cortical synaptic density. *Proc Natl Acad Sci U S A*. 2013;110(16):6571–6576.
90. Alvarez-Buylla A, Lim DA. For the long run: Maintaining germinal niches in the adult brain. *Neuron*. 2004;41(5):683–686.
91. Wurmser AE, Palmer TD, Gage FH. Cellular interactions in the stem cell niche. *Science*. 2004;304(5675):1253–1255.
92. Ohab JJ, Fleming S, Blesch A, Carmichael ST. A neurovascular niche for neurogenesis after stroke. *J Neurosci*. 2006;26(50):13007–13016.
93. Zacchigna S, Lambrechts D, Carmeliet P. Neurovascular signalling defects in neurodegeneration. *Nat Rev Neurosci*. 2008;9(3):169–181.
94. Bellucci A, Zaltieri M, Navarria L, Grigoletto J, Missale C, Spano P. From α -synuclein to synaptic dysfunctions: New insights into the pathophysiology of Parkinson's disease. *Brain Res*. 2012;1476(11):183–202.
95. Volpicelli-Daley LA, Luk KC, Patel TP, et al. Exogenous α -synuclein fibrils induce lewy body pathology leading to synaptic dysfunction and neuron death. *Neuron*. 2011;72(1):57–71.
96. Abbasi N, Fereshtehnejad SM, Zeighami Y, Larcher KMH, Postuma RB, Dagher A. Predicting severity and prognosis in Parkinson's disease from brain microstructure and connectivity. *Neuroimage Clin*. 2020;25:102111.
97. Pyatigorskaya N, Yahia-Cherif L, Valabregue R, et al. Parkinson disease propagation using MRI biomarkers and partial least squares path modeling. *Neurology*. 2021;96(3):e460–e471.
98. Kamagata K, Zalesky A, Hatano T, et al. Connectome analysis with diffusion MRI in idiopathic Parkinson's disease: Evaluation using multi-shell, multi-tissue, constrained spherical deconvolution. *Neuroimage Clin*. 2018;17:518–529.
99. Lee SJ, Desplats P, Sigurdson C, Tsigelny I, Masliah E. Cell-to-cell transmission of non-prion protein aggregates. *Nat Rev Neurol*. 2010;6(12):702–706.
100. Elston GN, Oga T, Fujita I. Spinogenesis and pruning scales across functional hierarchies. *J Neurosci*. 2009;29(10):3271–3275.
101. Borghammer P, Østergaard K, Cumming P, et al. A deformation-based morphometry study of patients with early-stage Parkinson's disease. *Eur J Neurol*. 2010;17(2):314–320.
102. Gorges M, Kunz MS, Müller HP, et al.; LANDSCAPE Consortium. Longitudinal brain atrophy distribution in advanced Parkinson's disease: What makes the difference in “cognitive status” converters? *Hum Brain Mapp*. 2020;41(6):1416–1434.
103. Lewis S, Foltynic T, Blackwell A, Robbins T, Owen A, Barker R. Heterogeneity of Parkinson's disease in the early clinical stages using a data driven approach. *J Neurol Neurosurg Psychiatry*. 2005;76(3):343–348.
104. Liu P, Feng T, Wang Y, Zhang X, Chen B. Clinical heterogeneity in patients with early-stage Parkinson's disease: A cluster analysis. *J Zhejiang Univ*. 2011;12(9):694–703.
105. Tremblay C, Achim AM, Macoir J, Monetta L. The heterogeneity of cognitive symptoms in Parkinson's disease: A meta-analysis. *J Neurol Neurosurgery and Psychiatry*. 2013;84(11):1265–1272.